

Structure of  $^{75}\text{Se}$ G. P. S. Sahota, V. K. Mittal, S. D. Sharma, H. S. Sahota, G. Singh,\* S. S. Datta,\*<sup>†</sup> and I. M. Govil\**Department of Physics, Punjabi University, Patiala 147002, India*

(Received 17 December 1990)

The low-lying low-spin levels of  $^{75}\text{Se}$  have been investigated. These levels were populated via the  $^{75}\text{As}(p, n\gamma)^{75}\text{Se}$  reaction with proton energies between 3.0 and 4.0 MeV. Angular distribution measurements have been used to assign spin values and to determine multipole mixing ratios via compound statistical theory of nuclear reactions. Lifetimes for 17 states in  $^{75}\text{Se}$  were obtained by the Doppler-shift attenuation method for the first time. For several of the transitions in  $^{75}\text{Se}$ , values or limits for  $B(M1)$  and  $B(E2)$  were obtained. The negative-parity sequence of levels up to about 2.5 MeV could be predicted well on the basis of the collective model with Coriolis perturbation. An effective moment-of-inertia parameter under the effect of Coriolis perturbation is used to predict these states. The results compare quite well with experimental values.

## I. INTRODUCTION

Though the  $^{75}\text{Se}$  nucleus has been investigated extensively both experimentally and theoretically in the past, the properties of many levels are yet uncertain. This is an exciting nucleus to investigate as odd neutron nuclei around  $N=40$  show low-lying anomalous  $\frac{7}{2}^+$  and  $\frac{5}{2}^+$  states in addition to the expected positive- and negative-parity states. Experimental information on  $^{75}\text{Se}$  mainly comes from the  $(p, n)$ ,  $(p, n\gamma)$ ,  $(\alpha, n\gamma)$ ,  $(d, p)$ , and  $(n, \gamma)$  reactions [1–5] and  $^{75}\text{Br}$  decay [6]. Theoretically, this nucleus has been investigated by many workers [7–13].

Testing of these theoretical predictions is hindered by a lack of experimental information, on both positive- and negative-parity levels arising from the coupling of  $2p_{3/2}$ ,  $1f_{5/2}$ , and  $2p_{1/2}$  single-particle shells. The available experimental information on  $^{75}\text{Se}$  has been compiled by Farhan and Rab [14]. From this compilation [14] it is clear that although the level scheme of  $^{75}\text{Se}$  has been well established, the lifetimes and spins of many states are still uncertain. It has been shown from the  $(\alpha, n\gamma)$  and  $(p, n)$  work that  $E2$  transitions from the low-lying states are highly enhanced, and so the measurement of  $B(E2)$  values for transitions from the higher levels will provide a direct and unambiguous measure of quadruple collectivity.

The purpose of the present study was to provide additional experimental data on the level structure of  $^{75}\text{Se}$  through the  $^{75}\text{As}(p, n\gamma)$  reaction, and to test critically the existing and the future theoretical models for this nucleus. In this work we have measured the lifetimes of levels using the Doppler-shift attenuation technique. The angular momentum and multipole mixing ratios were extracted from the angular distribution data. From these measured quantities the  $B(E2)$  and  $B(M1)$  transition probabilities for electric quadrupole and magnetic dipole components of various transitions with well-established  $J^\pi$  values are deduced.

Finally, the energy spectrum was generated theoretically on the basis of a collective model using Coriolis cou-

pling. The spectrum of negative-parity states was well reproduced on the basis of particle states  $\frac{1}{2}^- [550]$  and  $\frac{3}{2}^- [541]$ . However, positive-parity spectrum could not be properly accounted for by this approach.

## II. EXPERIMENTAL PROCEDURE

The experiment was performed using the Variable Energy Cyclotron at Chandigarh. A spectroscopically pure (99.999% pure),  $\sim 0.5\text{-mg/cm}^2$ -thick  $^{75}\text{As}$  target inclined at an angle of  $45^\circ$  with respect to the beam direction was exposed to a proton beam of different energies. Excitation functions were measured with a  $70\text{-cm}^3$  true coaxial HPGe detector with a resolution of about 1.8 keV for the 1332-keV  $^{60}\text{Co}$  line. For excitation functions and branching-ratio measurements, the detector was placed at 25 cm from the target and at an angle of  $55^\circ$  with respect to the beam axis. A graded filter consisting of Pd, Cu, and Al foils was placed in front of the detector to suppress low-energy gamma rays. Gamma-ray spectra were recorded at 3.0, 3.5, and 4.0 MeV proton energies. A  $2.5\text{ cm} \times 2.5\text{ cm}$  NaI(Tl) detector was located at  $270^\circ$  at a distance of 25 cm from the target to act as a monitor. Signals from the HPGe detector were analyzed using an ND77 4K channel multichannel pulse-height analyzer. The ND77 was coupled with a MICROVAX II computer for off-line analysis of the data. Electronic shifts in gain, if any, were monitored using photopeaks at 843, 1014, and 1461 keV. In order to obtain angular distributions of gamma rays, spectra were recorded at five angles between  $0^\circ$  and  $90^\circ$ . At each angle a number of spectra (five to ten) were recorded and those data with gain drift greater than 0.05 keV were rejected. Energy and efficiency calibrations were performed using  $^{56}\text{Co}$ ,  $^{75}\text{Se}$ ,  $^{110}\text{Ag}^m$ ,  $^{133}\text{Ba}$ ,  $^{152}\text{Eu}$ , and  $^{182}\text{Ta}$  radioactive sources. Gamma-ray spectra were analyzed using the computer code SAMPO of Routti and Prussian [15]. A typical gamma-ray spectrum at  $90^\circ$  with respect to the incident beam at 4.0 MeV is shown in Fig. 1. The gamma-ray energies are marked in the figure. The lines marked As

were identified as being due to either Coulomb excitation or the  $(p,p')$  reaction in  $^{75}\text{As}$ . Background peaks were identified by replacing the  $^{75}\text{As}$  target with natural spectroscopically pure C and Si targets.

Excitation functions of all observed gamma rays were analyzed carefully, and those from the  $(p,n)$  reaction were easily identified with a characteristic rise above their threshold energy. The excitation functions were thus used to check the origin of observed gamma rays.

### III. ANALYSIS OF DATA

The energies of the gamma rays were calculated from the spectra recorded at  $90^\circ$  and branching ratios were extracted from the singles spectra obtained with the detector at  $55^\circ$  with respect to the beam direction. Gamma-ray energies and branching ratios measured in the present work are shown in Table I.

Mean lifetimes were determined for many transitions

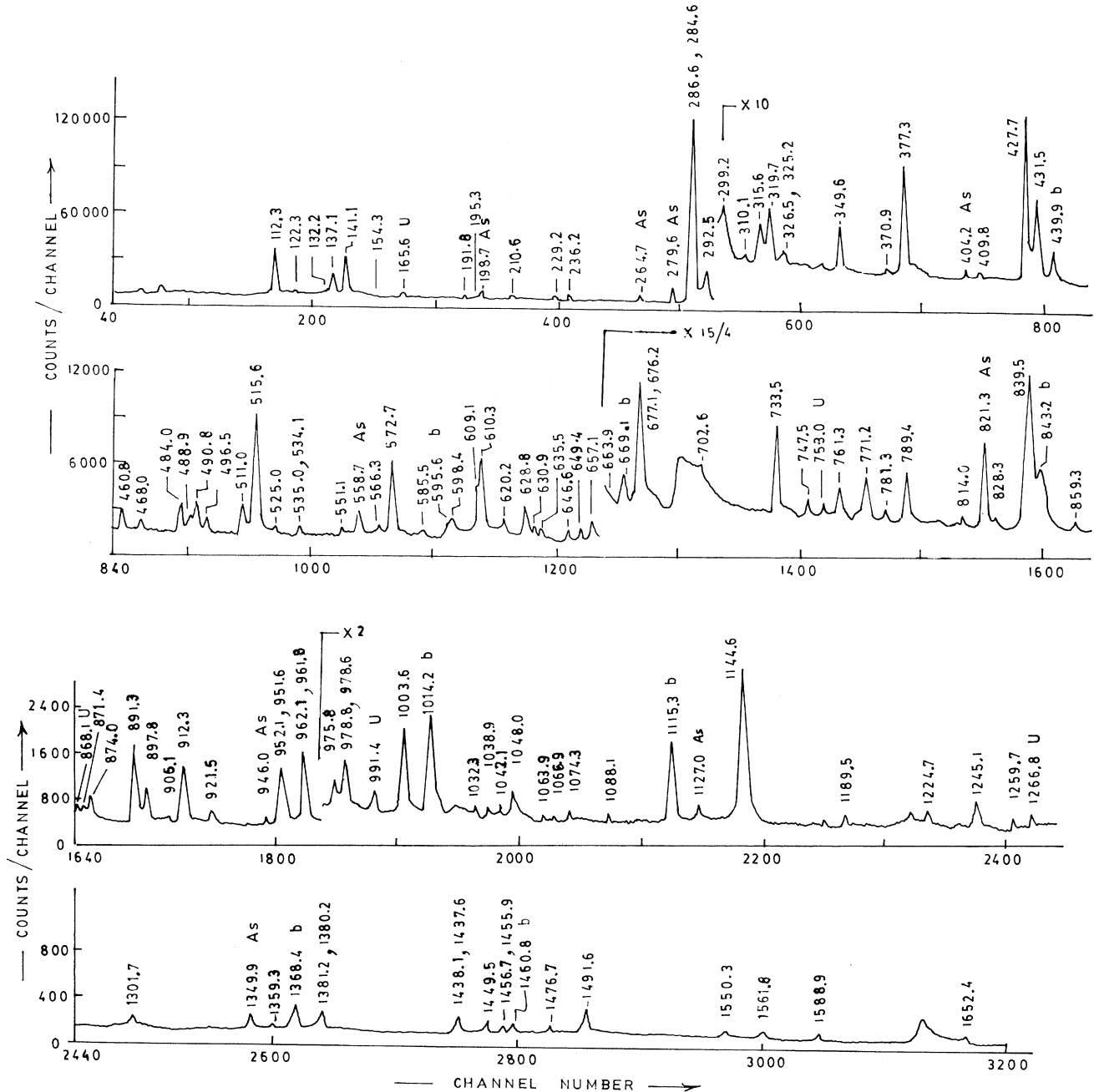


FIG. 1.  $\gamma$ -ray spectrum from the reaction  $^{75}\text{As}(p, n\gamma)$ ,  $^{75}\text{Se}$  at  $E_p = 4.0$  eV taken at  $90^\circ$  to the beam direction. The photopeaks labeled only by energy have been assigned to  $^{75}\text{Se}$ . Peaks labeled as As are due to the  $(p, p'\gamma)$  reaction of  $^{75}\text{As}$ . Peaks due to background or unidentified radiations are labeled b or u.

TABLE I. Summary of the level energies,  $J^\pi$  values,  $\gamma$ -ray energies, and branching ratios for transitions in  $^{75}\text{Se}$  determined in this work.

$J^\pi$	Initial level	Final level	$E_\gamma$	Branching ratios (%)	
				Present	Farhan and Rab [14]
$\frac{5}{2}^+$	0				
$\frac{7}{2}^+$	112.27(4)	0	112.27	100	100
$\frac{9}{2}^+$	132.24(9)	0	132.24	100	100
$\frac{3}{2}^-$	286.54(4)	0	286.54	100	100
		132.24	154.30	0.04	
$\frac{5}{2}^-$	427.70(4)	0	427.70	38.9(14)	35.8
		112.27	315.43	7.5(3)	6.4
		286.54	141.18	53.6(19)	57.8
$\frac{3}{2}^-$	585.48(6)	0	585.48	4.9(2)	5.5
		286.54	299.00	7.8(3)	9.1
		293.03	292.45	87.3(31)	85.4
$\frac{1}{2}^+$	610.34(11)	0	610.34	100	91.1
			324.13		0.2
			317.61		8.7
$\frac{5}{2}^+$	628.80(8)	0	628.80	22.4(8)	20.2
		112.27	515.55	71.0(25)	72.2
		132.24	496.53	6.6(2)	5.3
			341.86		2.3
$\frac{5}{2}^-$	663.91(4)	0	663.91	1.5(1)	1.2
		112.27	551.64	4.2(2)	5.7
		286.54	377.38	77.7(22)	77.6
		293.07	370.85	0.04	0.33
		427.70	236.22	16.6(6)	15.3
$\frac{7}{2}^-$	747.45(7)	0	747.45	9.1(3)	11.7
		112.27	635.19	8.7(3)	11.1
		286.54	460.91	23.5(9)	17.5
		427.70	319.75	66.3(22)	58.4
		610.34	137.11	2.4(1)	
		663.91	83.69		1.3
$\frac{5}{2}^-$	777.29(8)	0	777.29		2.1
		286.54	490.75	32.1(11)	34.0
		293.03	484.22	29.7(10)	25.9
		427.70	349.58	27.7(10)	26.5
		585.48	191.81	10.5(4)	10.2
		663.91	113.38		1.2
$\frac{7}{2}$	789.35(7)	0	789.35	74.8(26)	47.9
		112.27	677.08	1.7	37.3
		132.24	657.08	23.5(8)	13.4
		628.80	161.56		1.4
$\frac{7}{2}, \frac{9}{2}$	839.51(7)	0	839.51	76.3(23)	73.2
		112.27	727.24		2.9
		610.34	229.19	6.8(2)	7.5
		628.80	210.71	16.9(6)	16.5
$\frac{3}{2}^-$	859.25(8)	0	859.25	2.8(1)	4.0
		286.54	572.74	33.6(12)	30.6
		293.03	566.26	5.1(2)	6.7
		427.70	431.56	57.1(20)	55.6
		628.80	231.11		0.97
		663.91	195.34	1.4(1)	2.2
$\frac{1}{2}^-, \frac{3}{2}^-$	895.61(5)	286.54	609.12	79.2(28)	84.5
		427.70	467.95	16.2(6)	5.2
		585.48	310.13	4.6(2)	5.1
		610.34	284.56		6.0
	952.06(4)	0	952.06	97.7(145)	47.4
		112.27	839.85		28.4

TABLE I. (*Continued*).

$J^\pi$	Initial level	Final level	$E_\gamma$	Branching ratios (%)		
				Present	Farhan and Rab [14]	
$\frac{3}{2}^-$	961.82(10)	132.24	819.82		15.6	
		427.70	524.36	2.3(1)		
		777.29	174.77		8.5	
		0	961.82	40.9(14)	35.2	
		286.54	675.21	51.1(18)	43.5	
		292.29	669.53		5.0	
		427.70	534.16	7.0(11)	6.7	
		585.48	376.34		1.5	
		628.80	333.02		1.3	
		663.91	297.91		5.3	
$\frac{3}{2}^+, \frac{5}{2}^+$	1003.64(8)	839.51	122.30	1.0(1)	1.4	
		0	1003.64	33.7(12)	45.5	
		112.27	891.34	55.0(20)	50.6	
		132.24	871.43	11.3(4)	2.27	
$\frac{1}{2}^-, \frac{3}{2}^-$	1020.08(4)	628.80	374.84		1.7	
		286.54	733.57	96.7(34)	100	
		610.34	409.79	3.3(1)		
$\frac{5}{2}^-, \frac{7}{2}^-$	1047.94(4)	0	1047.94	22.7(30)		
		286.54	761.40	30.0(11)	13.0	
$\frac{5}{2}^-$	1073.82(5)	427.70	620.24	47.3(17)	87.0	
		0	1073.82	10.0(4)	6.5	
		112.27	961.55	51.7(75)	43.0	
		293.03	780.79	14.2(5)	8.9	
		427.70	646.09	6.0(2)	15.2	
		585.48	488.35	18.0(6)	13.8	
		747.81	326.02	0.4	12.7	
		789.35	284.47	0.4		
$\frac{7}{2}^+$	1087.12(4)	0	1087.12	7.4(3)		
		112.27	974.85	92.6(31)		
$\frac{3}{2}^+, \frac{5}{2}^+$	1144.59(7)	0	1144.59	97.0(32)	100	
		112.27	1032.32	3.0(1)		
		286.54	897.84	35.9(13)	67.3	
		585.48	598.96	43.9(15)	22.9	
$\frac{5}{2}^-$	1198.90(5)	859.25	325.16	20.2(30)	9.8	
		286.54	912.33	54.5(19)	63.7	
		427.70	771.23	30.0(11)	29.3	
		663.91	535.0	15.5(6)	7.0	
		0	1245.10	100	20.57	
$\frac{3}{2}^-, \frac{5}{2}^-, \frac{7}{2}^-$	1245.10(6)	286.54	958.56		6.9	
		293.07	952.04	0.1	60.5	
		585.48	659.62	0.1	12.1	
		0	1259.68	20.2(7)	39.4	
		628.8	630.87	79.8(28)	60.61	
		0	1301.73	25.5(9)	21.4	
$\frac{5}{2}^+, \frac{7}{2}^+$	1301.73(8)	112.27	1189.50	4.2(2)	28.8	
		427.70	874.03	70.3(25)	49.8	
		1380.18(12)	0	1380.18	100(14)	100
		1406.37(11)	427.70	978.67	100(14)	100
$\frac{7}{2}^+$	1438.74(10)	0	1438.74	27.5(10)	100	
		789.35	649.40	72.5(25)		
$\frac{5}{2}^-$	1455.90(8)	0	1455.90	11.5(4)		
		585.48	870.42	88.5(31)	100	
		0	1491.56	83.0(29)	100	
$\frac{7}{2}^+$	1491.56(6)	132.24	1359.31	4.5(2)		
		427.70	1063.86	6.8(2)		
		585.48	906.08	5.7(2)		

TABLE I. (Continued).

$J^\pi$	Initial level	Final level	$E_\gamma$	Branching ratios (%)	
				Present	Farhan and Rab [14]
$\frac{7}{2}^+, \frac{9}{2}^+$	1550.32(12)	0	1550.32	30.6(11)	
		112.27	1438.01	41.4(15)	
		628.80	921.52	28.0(11)	
$\frac{7}{2}^-$	1561.83(6)	0	1561.83	5.5(2)	20.6
		112.27	1449.54	18.8(7)	29.4
		585.48	976.35		40.3
		747.81	814.02	11.7(4)	
		859.25	702.57	64.0(23)	9.7
		1588.93(10)	0	1588.93	9.4(3)
$\frac{5}{2}$	1652.41(7)	112.27	1476.68	10.7(4)	
		132.24	1456.69	3.6(1)	
		610.34	978.60	76.3(114)	100
		0	1652.41	38.4(13)	
		427.70	1224.70	21.6(8)	
$\frac{5}{2}^-$	1667.72(7)	585.48	1066.93	17.9(6)	
		610.34	1042.08	22.1(8)	
		286.54	1381.18	51.5(77)	
		628.80	1038.92	21.6(8)	
		839.51	828.21	26.9(10)	

using Doppler-shift attenuation (DSA) technique from the single gamma-ray spectra obtained at various angles between  $0^\circ$  and  $90^\circ$ . As the observed shifts are small because of the low recoil velocity, spectra were accumulated with internal standards. The centroids of photopeaks at different angles were plotted versus  $\cos\theta$  and are shown in Fig. 2. The experimental values of the attenuation factors  $F(\tau)$  were calculated from the slope of this straight line. The theoretical  $F(\tau)$ -vs- $\tau$  curve was constructed using the theory of Lindhard, Scharff, and Schiott (LSS) [16] for stopping along with the Blaugrund [17] correction for atomic scattering. Further details of the method of analysis of DSA data are given in our earlier publications [18,19]. The values of the measured lifetimes of various levels are given in Table II along with their respective experimental  $F(\tau)$  values.  $F(\tau)$  values are given at  $E_p = 4.0$  MeV, but lifetimes are weight-averaged, values at  $E_p = 3.0$  and 4.0 MeV.

The gamma-ray angular distribution data were used to extract the coefficients  $A_2$  and  $A_4$  by a least-squares fit with the expression

$$W(\theta) = 1 + A_2 Q_2 P_2(\cos\theta) + A_4 Q_4 P_4(\cos\theta).$$

The geometrical attenuation factors  $Q_2$  and  $Q_4$  were taken to be unity because of the large detector-to-target distance. Theoretically,  $A_2$  and  $A_4$  coefficients were generated using the computer code CINDY written by Sheldon and Rogers [20]. For transmission coefficient calculations we used two sets of optical-model parameters first by Rosen, Beery, and Goldhaber [21] for protons and Wilmore and Hodgson [22] for neutrons, and second a set given by Perey [23] and Moldauer [24]. Orbital angular momentum for the incoming and outgoing channels was restricted to  $l = 4$ . In these calculations elastic and all possible proton inelastic, proton capture, and neutron

exit channels for the compound nucleus were included. However, the inclusion of proton capture and proton inelastic exit channels was found to contribute very little toward the structure of angular distribution curves. Further, the structures of the angular distribution curves were found to be identical for the two different sets of optical-model parameters. Thus we used the first set of optical-model parameters in our calculations. The method of analysis of angular distribution data has been described earlier [19]. Figure 3 contains the experimental angular distributions for some of the observed transitions, together with theoretical curves for different assumed spin values of the decaying state and respective  $\chi^2$  curves. Initial spin values were considered in a range permitted by the mode of decay of the state under consideration, the lifetime of the state, and the probable spin quoted in literature. The 0.1% confidence limit was used to exclude unacceptable fits. The experimental  $A_2$  and  $A_4$  coefficients obtained are shown in Table III together with spin values and multipole mixing ratios. The phase convention of Rose and Brink [25] was employed throughout the analysis. The present results are compared with the values available in literature [14]. The adopted values in the last column of Table III are weighted averages of all the measurements.

#### IV. RESULTS

The excitation energies of various levels in  $^{75}\text{Se}$  were determined and compared with earlier measurements [5,14]. In general, the level energies measured in the present work are in good agreement with earlier measured values [5,14]. However, in certain cases, there are discrepancies, as large as 1 keV, but our measured energies are more close to  $(p,n)$  work [1,2]. The branching ratios for various transitions are also compared with the

values available in literature [14]. In some cases we could not observe very weak transitions, but the overall agreement is quite good. Spin values for most of the levels are consistent with previously assigned values [14]. However, in some cases there are certain discrepancies which we shall discuss below.

tion [14] this level was reported to have  $\frac{1}{2}, \frac{3}{2}$  as probable spin. However, present data favors  $\frac{5}{2}$  as the more probable spin for this level. The lifetime of this level is found to be  $180^{+240}_{-80}$  fs.

**A. Level at 1199 keV**

Angular distributions of the 912- and 771-keV gamma rays deexciting this level predict  $\frac{5}{2}$  as the probable spin for this level. The mixing ratios for 1199→286 and 1198→427 keV transitions are  $-0.09(2)$  or  $-2.50(15)$  and  $0.11(1)$  or  $1.23(11)$ , respectively. In a recent compila-

**B. Level at 1245 keV**

This level was reported [14] to have spin  $\frac{3}{2}$ . However, the angular distribution of the 1245-keV gamma ray predicts  $\frac{5}{2}, \frac{7}{2}$  as the probable spin for this level, though the present data could not rule out the spin assignment of  $\frac{3}{2}$ . The lifetime of this state is found to be  $360^{+1900}_{-150}$  fs.

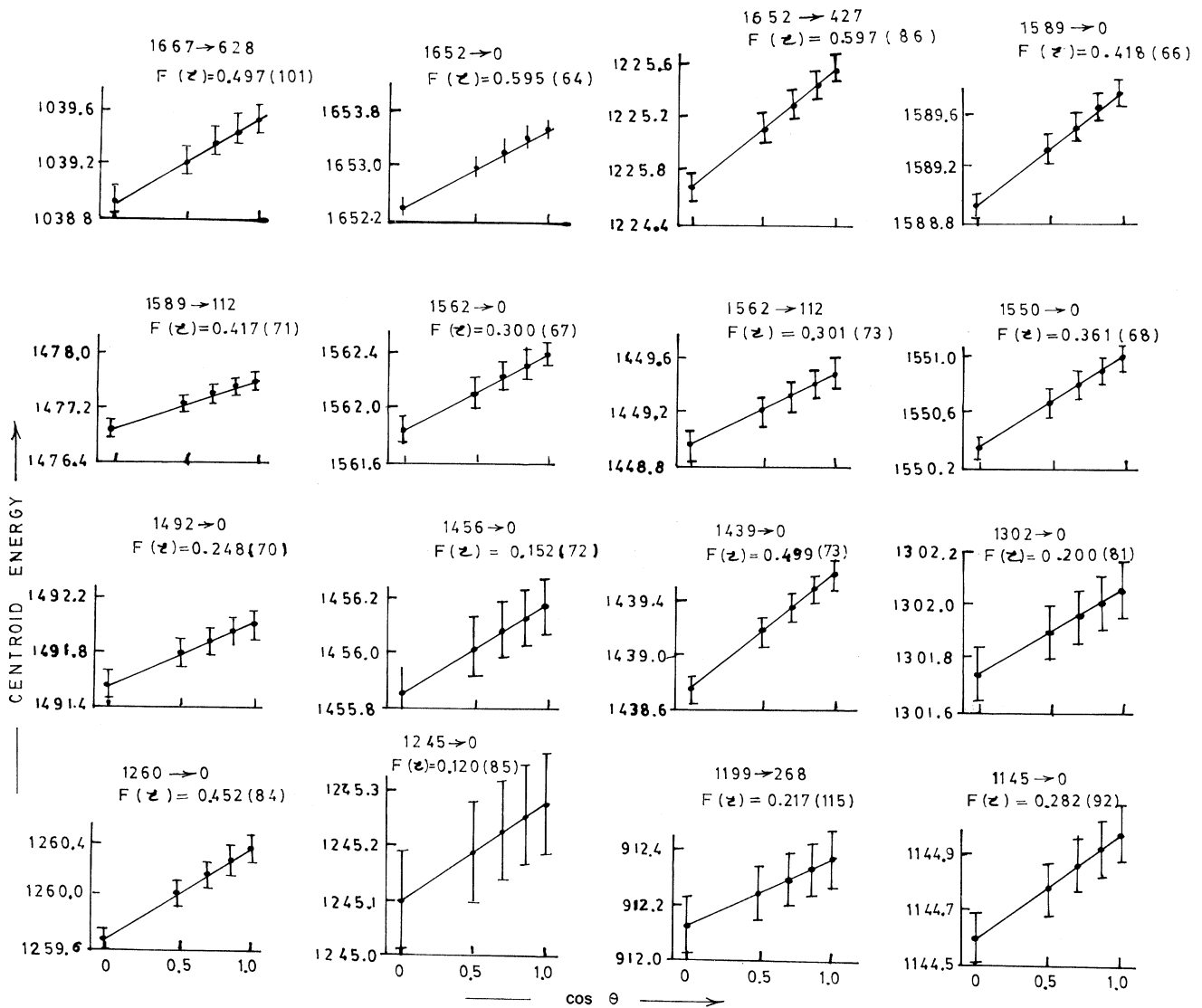


FIG. 2. Plots of the centroid energy in keV for some indicated  $\gamma$  rays from  $^{75}\text{Se}$  observed in single measurements vs  $\cos\theta$ .  $F(\tau)$  values given are at  $E_p = 4.0$  MeV.

TABLE II. Summary of the lifetimes for levels in  $^{75}\text{Se}$  determined by Doppler-shift attenuation method from centroid measurements in singles experiments.  $F(\tau)$  are given at  $E_p = 4.0$  MeV, whereas  $\tau$  is the weight-averaged values at  $E_p = 3.0$  and  $E_p = 4.0$  MeV.

$E_{\text{level}}$	$E_\gamma$	$F(\tau)$	Weighted $\overline{F(\tau)}$	$\tau$ (fs)
1003.64	1003.64	0.400(105)	0.400(105)	$78^{+42}_{-26}$
1047.94	1047.94	0.242(100)	0.242(100)	$160^{+140}_{-40}$
1074.33	1074.33	0.327(98)	0.327(98)	$105^{+65}_{-35}$
1088.11	975.03	0.142(108)	0.142(108)	$300^{+1500}_{-150}$
1144.59	1144.59	0.282(92)	0.282(92)	$128^{+82}_{-40}$
1198.90	912.13	0.217(115)	0.217(115)	$180^{+240}_{-80}$
1245.10	1245.10	0.120(85)	0.120(85)	$360^{+1000}_{-150}$
1259.68	1259.68	0.452(84)	0.452(84)	$64^{+26}_{-17}$
1301.73	1301.73	0.200(81)	0.200(81)	$200^{+150}_{-70}$
1438.74	1438.74	0.499(73)	0.499(73)	$54^{+18}_{-12}$
1455.90	1455.90	0.152(72)	0.152(72)	$270^{+260}_{-100}$
1491.56	1491.56	0.248(70)	0.248(70)	$150^{+80}_{-40}$
1550.32	1550.32	0.361(68)		
			0.361(52)	$92^{+30}_{-24}$
	1437.01	0.360(80)		
1561.83	1561.83	0.300(67)		
			0.301(49)	$120^{+45}_{-30}$
	1448.94	0.301(73)		
1588.93	1588.93	0.418(66)	0.418(48)	$72^{+22}_{-12}$
	1476.88	0.417(71)		
1652.41	1652.41	0.595(64)		
			0.596(51)	$38^{+20}_{-10}$
	1224.65	0.597(86)		
1667.72	1038.92	0.497(101)	0.497(101)	$54^{+26}_{-17}$

### C. Level at 1491 keV

The lifetime of this level extracted in the present measurements is  $150^{+80}_{-40}$  fs. This level was reported [14] to decay to ground state only. But the present work clearly indicates that there are three more weak transitions from this level. The observed branching ratios for this level are  $1491 \rightarrow 0$  (83.0%),  $1491 \rightarrow 133$  (4.5%),  $1491 \rightarrow 427$  (6.8%), and  $1491 \rightarrow 585$  (5.7%). The angular distribution of the 1491-keV gamma ray from the  $1491 \rightarrow 0$  keV transition predicts  $\frac{7}{2}$  to be the spin of this level, with a mixing ratio of 0.29(4) or  $-1.60$ (14).

### D. Level at 1561 keV

The lifetime of this level is  $120^{+45}_{-30}$  fs. The present experiment predicts the decay mode of this level as  $1561 \rightarrow 0$  (5.5%),  $1561 \rightarrow 112$  (18.8%),  $1561 \rightarrow 747$  (11.7%), and  $1561 \rightarrow 859$  (64.0%). The transition to the 586-keV level reported earlier [14] could not be confirmed in our experiment. The spin of this level was earlier [14] reported as  $\frac{3}{2}, \frac{5}{2}$ . However, our experiment rules out the possibility of  $\frac{3}{2}, \frac{5}{2}$  as spin for this level. The angular distribution of the 701-keV gamma ray deexciting this level predicts  $\frac{7}{2}$  as the most probable spin for this level. The mixing ratio for this transition is 0.19(6).

### E. Level at 1667 keV

This level was reported in ( $p, n$ ) work [2], but it was not seen in recent ( $\alpha, n$ ) and ( $n, \gamma$ ) works [3,5]. In ( $p, n$ ) work

[2] this level was reported to decay 100% to the 286-keV state. In the present experiment, we again propose this level. This level is found to decay via three branches; the respective transitions are  $1667 \rightarrow 286$  (51.5%),  $1667 \rightarrow 627$  (21.6%), and  $1667 \rightarrow 839$  (26.9%). The angular distributions of the 1380- and 1038-keV transitions deexciting this level predict the spin of this level to be  $\frac{5}{2}$ . The lifetime of this level is  $54^{+26}_{-17}$  fs.

Considering the lifetimes and decay modes of the various levels, the levels at 1550, 1491, 1438, 1259, 1144, and 1088 keV can be assigned positive parity since a negative parity will result in enhanced  $B(M2)$  values which are uncommon in this mass region. Similarly, the levels at 1667, 1562, 1455, 1198, and 1047 keV can be assigned negative parity since a positive parity will again result in enhanced  $B(M2)$  values. From the measured branching ratios, level lifetimes, and multipole mixing ratios presented in Tables I–III, the reduced transition probabilities for many of the transitions in  $^{75}\text{Se}$  were calculated. These values are summarized in Table IV. The  $B(E2)$  and  $B(M1)$  values are given in Weisskopf units.

## V. DISCUSSION

Since almost all the transitions are enhanced, as is evident from Table IV, it is inferred that the nucleus is highly deformed. This conclusion is confirmed from the fact that the quadrupole moment of this nucleus [26] is 1.0 b, which yields  $\beta \approx 0.35$ . This value of  $\beta$  is in agreement with the value of  $\beta$  used by Agarwal *et al.* [1]. The large

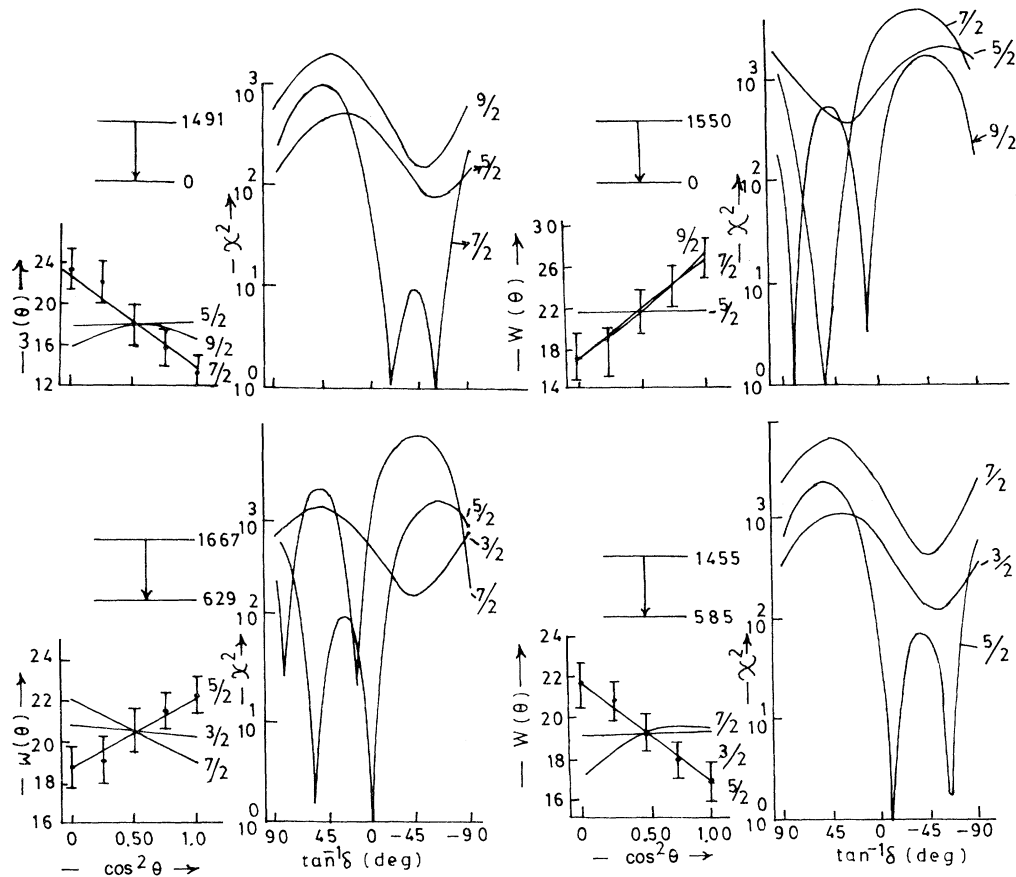


FIG. 3. Typical results of the angular distribution curves together with  $\chi^2$  as a function of dipole/quadrupole mixing parameter  $\arctan\delta$  for some transitions in  $^{75}\text{Se}$ .

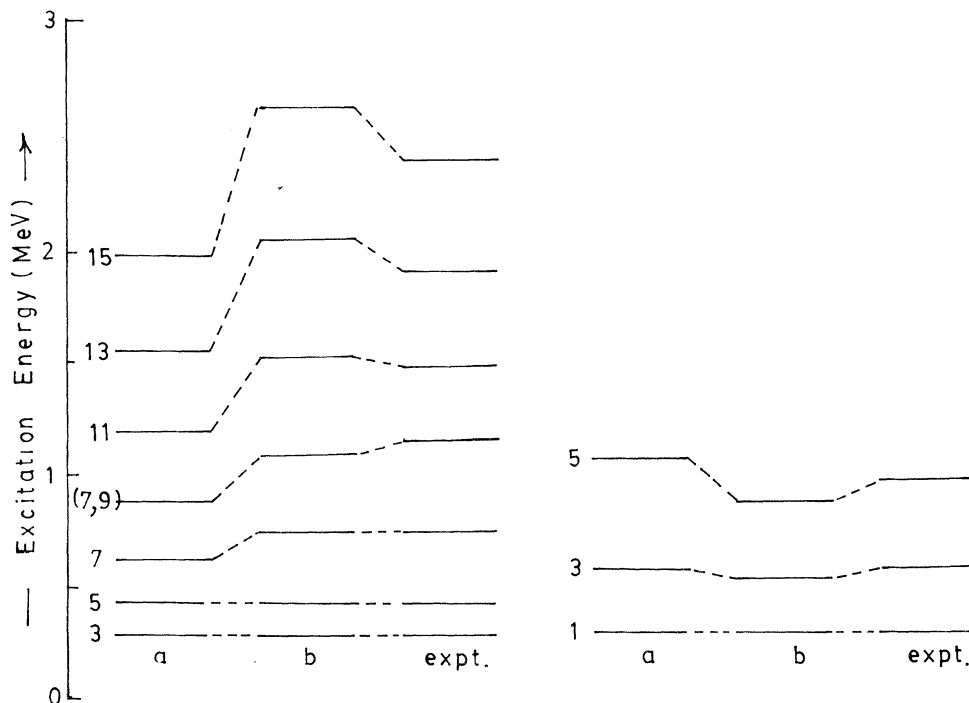


FIG. 4. The two lowest-energy negative-parity bands based on  $\frac{3}{2}^- [541]$  and  $\frac{1}{2}^- [550]$  bands in  $^{75}\text{Se}$  compared with predictions of collective models with Coriolis coupling. Twice the spins are given. *a* refers to theoretical predictions without Coriolis coupling, while *b* refers to the predictions with Coriolis coupling.

quadrupole moment of  $^{75}\text{Se}$  suggests deformation  $\beta \geq 0.35$ . In prior work the positive- and negative-parity states in the level scheme up to  $\sim 2$  MeV could not be explained satisfactorily.

The lowest-energy negative-parity bands are based on  $\frac{1}{2}^- [550]$  and  $\frac{3}{2}^- [541]$ . These are Coriolis coupled. In

our analysis these perturbed bands are generated on an approach based on an effective moment-of-inertia parameter under Coriolis perturbations. The effective moment-of-inertia parameter is obtained by diagonalizing the collective Hamiltonian with rotating core and off-diagonal Coriolis terms. In this treatment eigenvectors

TABLE III. Summary of angular distribution analysis for  $E_p = 4.0$  MeV.

Transition	$A_2$	$A_4$	Present work	Mixing ratio $\delta$ Farhan and Rab [14]	Adopted
$112(\frac{7}{2}) \rightarrow 0(\frac{5}{2})$	-0.360(22)	0.001(34)	-0.24(5)	-0.27(6)M1+E2	-0.25(4)
$133(\frac{9}{2}) \rightarrow 0(\frac{5}{2})$	0.332(50)	-0.077(55)	E2	E2	E2
$428(\frac{5}{2}) \rightarrow 0(\frac{5}{2})$	-0.082(41)	0.002(52)	E1	E1	E1
$\rightarrow 287(\frac{3}{2})$	-0.368(32)	0.094(41)	-0.11(9)	-0.19(10)M1+E2	-0.146(67)
$586(\frac{3}{2}) \rightarrow 293(\frac{1}{2})$	-0.071(31)	0.009(45)	-0.07(8) or -4.5(9)	0.14(7)M1+E2	-0.07(8) or -4.5(9)
$629(\frac{5}{2}) \rightarrow 0(\frac{5}{2})$	0.091(20)	0.020(21)	0.07(6) or 1.5(3)		0.07(6) or 1.5(3)
$\rightarrow 112(\frac{7}{2})$	0.011(20)	0.012(20)	M1	M1	M1
$664(\frac{5}{2}) \rightarrow 287(\frac{3}{2})$	-0.241(22)	0.006(22)	-0.75(18)	-0.7(5) M1+E2	0.744(169)
$\rightarrow 428(\frac{5}{2})$	0.091(21)	0.004(22)	0.07(6) or 2.0(5)		0.07(6) or 2.0(5)
$747(\frac{7}{2}) \rightarrow 428(\frac{5}{2})$	0.250(36)	0.022(36)	1.38(10)		1.38(10)
$777(\frac{5}{2}) \rightarrow 287(\frac{3}{2})$	-0.034(5)	-0.002(5)	0.08(2) or 3.49(9)		0.08(2) or 3.49(9)
$\rightarrow 428(\frac{5}{2})$	0.031(4)	0.005(4)	3.27(9)		3.27(9)
$789(\frac{7}{2}) \rightarrow 0(\frac{5}{2})$	-0.317(45)	-0.022(47)	0.84(6)		0.84(6)
$839(\frac{7}{2}, \frac{9}{2}) \rightarrow 0(\frac{5}{2})$	0.263(37)	0.024(38)	1.42(33)J = $\frac{7}{2}$ 0.12(2)J = $\frac{9}{2}$		1.43(33)J = $\frac{7}{2}$ 0.12(2)J = $\frac{9}{2}$
$1047(\frac{5}{2}, \frac{7}{2}) \rightarrow 0(\frac{5}{2})$	-0.047(6)	-0.006(6)	0.09(2)J = $\frac{7}{2}$ > 23J = $\frac{5}{2}$		0.09(2)J = $\frac{7}{2}$ > 23J = $\frac{5}{2}$
$\rightarrow 287(\frac{3}{2})$	0.140(20)	-0.004(20)	0.78(5) or 2.74(10)J = $\frac{5}{2}$		0.78(5) or 2.74(10)J = $\frac{5}{2}$
$\rightarrow 427(\frac{5}{2})$	-0.220(32)	-0.016(33)	0.22(7) or 2.36(11)J = $\frac{7}{2}$		0.22(7) or 2.36(11)J = $\frac{7}{2}$
$1088(\frac{7}{2}) \rightarrow 112(\frac{7}{2})$	0.161(23)	0.010(23)	0.06(7) or 0.96(10)		0.06(7) or 0.96(10)
$1144(\frac{5}{2}) \rightarrow 0(\frac{5}{2})$	0.116(17)	0.008(17)	0.07(2) or 1.33(15)		0.07(2) or 1.33(15)
$1198(\frac{5}{2}) \rightarrow 286(\frac{3}{2})$	-0.118(17)	-0.008(17)	-0.09(2) or -2.50(15)		-0.09(2) or -2.50(15)
$\rightarrow 427(\frac{5}{2})$	-0.101(14)	-0.007(15)	0.11(1) or 1.23(11)		0.11(1) or 1.23(11)
$1245(\frac{5}{2}, \frac{7}{2}) \rightarrow 0(\frac{5}{2})$	0.151(22)	0.010(22)	0.28(7) or 0.73(11)J = $\frac{5}{2}$ 4.01(11)J = $\frac{7}{2}$		0.28(7) or 0.73(11)J = $\frac{5}{2}$ 4.01(11)J = $\frac{7}{2}$
$1259(\frac{5}{2}, \frac{7}{2}) \rightarrow 0(\frac{5}{2})$	-0.285(41)	-0.021(43)	-0.27(7) or -1.88(11)J = $\frac{7}{2}$		-0.27(7) or -1.88(11)J = $\frac{7}{2}$
$\rightarrow 629(\frac{5}{2})$	-0.049(7)	-0.003(7)	> 10J = $\frac{5}{2}$ 0.07(3)J = $\frac{7}{2}$		> 10J = $\frac{5}{2}$ 0.07(3)J = $\frac{7}{2}$
$1301(\frac{5}{2}, \frac{7}{2}) \rightarrow 0(\frac{5}{2})$	-0.244(35)	-0.018(37)	-0.21(3) or -2.48(11)J = $\frac{7}{2}$		-0.21(3) or -2.48(11)J = $\frac{7}{2}$
$\rightarrow 427(\frac{5}{2})$	-0.068(9)	-0.004(10)	-0.74(7) or -6.04(22)J = $\frac{5}{2}$ 0.05(5)J = $\frac{7}{2}$		-0.74(7) or -6.04(22)J = $\frac{5}{2}$ 0.05(5)J = $\frac{7}{2}$
$1438(\frac{7}{2}) \rightarrow 0(\frac{5}{2})$	0.240(34)	0.040(34)	2.90(10)		2.93(10)
$\rightarrow 789(\frac{7}{2})$	0.145(23)	-0.029(25)	-1.52(34)		-1.52(34)
$1455(\frac{5}{2}) \rightarrow 585(\frac{3}{2})$	-0.166(23)	-0.012(24)	-0.20(2) or -1.88(9)		-0.20(2) or -1.88(9)
$1491(\frac{7}{2}) \rightarrow 0(\frac{5}{2})$	-0.334(48)	-0.011(50)	0.29(4) or -1.60(14)		0.29(4) or -1.60(14)
$1550(\frac{7}{2}, \frac{9}{2}) \rightarrow 0(\frac{5}{2})$	0.337(48)	0.032(48)	1.20(22)J = $\frac{7}{2}$ 4.7(1)J = $\frac{9}{2}$		1.20(22)J = $\frac{7}{2}$ 4.7(1)J = $\frac{9}{2}$
$\rightarrow 112(\frac{7}{2})$	-0.069(10)	-0.011(10)	0.73(5) or 9.50(10)J = $\frac{7}{2}$		0.73(5) or 9.50(10)J = $\frac{7}{2}$
$\rightarrow 629(\frac{5}{2})$	0.021(3)	0.003(3)	0.21(4)J = $\frac{7}{2}$		0.21(4)J = $\frac{7}{2}$
$1562(\frac{7}{2}) \rightarrow 859(\frac{3}{2})$	0.216(31)	0.001(31)	0.19(6)		0.19(6)
$1652(\frac{5}{2}) \rightarrow 0(\frac{5}{2})$	-0.027(3)	-0.003(4)	0.50(8)		0.50(8)
$\rightarrow 427(\frac{5}{2})$	0.118(17)	0.008(17)	0.04(4) or 1.60(10)		0.04(4) or 1.60(10)
$\rightarrow 610(\frac{1}{2})$	0.154(21)	0.001(22)	0.07(3) or -4.0(1)		0.07(3) or -4.0(1)
$1667(\frac{5}{2}) \rightarrow 286(\frac{3}{2})$	0.189 (27)	0.012(27)	0.74(4)		0.74(4)
$\rightarrow 629(\frac{5}{2})$	0.121(17)	0.008(17)	0.05(3) or 1.51(7)		0.05(3) or 1.51(7)

TABLE IV. Summary of the electromagnetic properties in  $^{75}\text{Se}$ .

Transition	Transition energy (keV)	$\tau$ (fs)	Branching ratio (%)	Mixing ratio $\delta$	$B(E2)$ (W.u.)	$B(M1)$ (mW.u.)
$122(\frac{7}{2}) \rightarrow 0(\frac{5}{2})$	112	0.69 ns <sup>a</sup>	100	-0.27(6)		125(25)
$133(\frac{7}{2}) \rightarrow 0(\frac{5}{2})$	133	5.3 ns <sup>a</sup>	100	$E2$		34(6)
$1047(\frac{5}{2}, \frac{7}{2}) \rightarrow 0(\frac{5}{2})$	1047	$160^{+140}_{-40}$	22.7	0.09(2) <sup>b</sup>		0.39(24)
$\rightarrow 286(\frac{3}{2})$	761		30.0	0.78(5) <sup>b</sup> or		
120.7(752)	84.0(524)			2.74(10)		281.6(1755)
$\rightarrow 428(\frac{5}{2})$	620		67.3	0.22(7) <sup>b</sup>		64.7(404)
$1088(\frac{7}{2}) \rightarrow 112(\frac{7}{2})$	976	$300^{+1500}_{-150}$	92.6	0.06(7) or	0.55(303)	105(500)
				0.96(10)		72.6(547)
$1144(\frac{5}{2}) \rightarrow 0(\frac{5}{2})$	1144	$128^{+82}_{-40}$	97.0	0.07(2) or	0.82(38)	160.0(750)
				1.33(15)		107.3(503)
$1198(\frac{5}{2}) \rightarrow 286(\frac{3}{2})$	912	$180^{+240}_{-80}$	54.5	-0.09(2) or	1.67(71)	125.7(589)
				-2.50(15)		179.7(842)
$\rightarrow 427(\frac{5}{2})$	771		30.3	0.11(1) or	3.17(148)	114.1(535)
				1.23(11)		160.0(745)
$1259(\frac{5}{2}, \frac{7}{2}) \rightarrow 0(\frac{5}{2})$	1259	$64^{+26}_{-17}$	20.2	-0.27(7) <sup>b</sup> or	2.94(100)	46.8(161)
				-1.88(11)		33.8(116)
$\rightarrow 629(\frac{5}{2})$	631		79.8	0.07(3) <sup>b</sup> or	26.4(91)	1568(540)
				> 10 <sup>b</sup>		< 5000
$1438(\frac{7}{2}) \rightarrow 0(\frac{5}{2})$	1438	$54^{+18}_{-12}$	27.5	2.90(10)		32.2(135)
$1455(\frac{5}{2}) \rightarrow 585(\frac{3}{2})$	870	$270^{+260}_{-100}$	88.5	-0.20(2) or	10.98(720)	151.9(1100)
				-1.88(9)		222.6(1522)
$1491(\frac{7}{2}) \rightarrow 0(\frac{5}{2})$	1491	$150^{+80}_{-40}$	83.0	0.29(4) or	23.5(10)	14.8(195)
				-1.60(14)		2.53(935)
$1550(\frac{7}{2}) \rightarrow 0(\frac{5}{2})$	1550	$92^{+30}_{-24}$	30.6	1.20(22)		9.50(314)
$\rightarrow 112(\frac{7}{2})$	1438		41.4	0.73(5) or	11.1(37)	31.4(104)
				9.5(1)		31.4(104)
$\rightarrow 628(\frac{5}{2})$	922		28.0	0.21(4)		8.38(278)
$1562(\frac{7}{2}) \rightarrow 859(\frac{3}{2})$	702	$120^{+45}_{-30}$	64.0	0.19(6)		1300(435)
$1667(\frac{5}{2}) \rightarrow 286(\frac{3}{2})$	1381	$54^{+26}_{-17}$	51.5	0.74(4)		29.2(119)
$\rightarrow 628(\frac{5}{2})$	1039		21.6	0.05(3) or	0.36(15)	113(46)
				1.51(7)		99.8(408)

<sup>a</sup>Lifetimes are taken from Ref. [14].

<sup>b</sup> $J = \frac{5}{2}$ .

obtained in single-particle Nilsson calculations are used to evaluate the decoupling parameter [27] (partial or total depending upon whether  $\Omega \neq \frac{1}{2}$  or  $= \frac{1}{2}$ ). The expression for effective moment-of-inertia parameter is

$$A' = A \left[ 1 + \frac{(2K+1)q}{I(I+1) - 2K + J(J+1)} \right],$$

where

$$q = -1 \pm \left[ 1 + \frac{\langle Hc \rangle^2}{(2K+1)^2} \right]^{1/2},$$

$\langle Hc \rangle$  being the matrix elements of the Coriolis part of the Hamiltonian in terms of  $a$  and  $I$ . The above expression is in a compact form obtained by manipulating the results from diagonalization of the Hamiltonian. In actual computations the unperturbed moment-of-inertia parameter is obtained from the lowest rotational energy gap, since the Coriolis perturbation is the lowest in this case.

The proposed  $\frac{1}{2}^-$ [550] and  $\frac{3}{2}^-$ [541] negative-parity bands are generated using this model. The results are compared with the experimental values as shown in Fig. 4. As is evident from the diagram, the spectrum of the lowest-energy negative-parity band is quite well reproduced on the basis of particle states  $\frac{3}{2}^-$ [541]. Earlier, we also tried the states  $\frac{3}{2}^-$ [532],  $\frac{3}{2}^-$ [521],  $\frac{3}{2}^-$ [512], and  $\frac{3}{2}^-$ [501], but with little success. Thus the state is  $\frac{3}{2}^-$ [541]. It is also justifiable from the fact that the energy of the particle is minimum in the state  $\frac{3}{2}^-$ [541] for deformation  $\beta \approx 0.35$ . Accordingly, this is the first available state to the particle which could generate the spectrum well. It may be noted that the Coriolis effect goes on increasing with spin, resulting in an increased moment of inertia at higher spins. As is clear from Fig. 4, the results compare well with experimental values up to 2 MeV or so. The discrepancy is about 100 keV for the spin  $\frac{13}{2}$  at energy  $\approx 2$  MeV, while the discrepancy with no Coriolis perturbation comes out to be very large, of the order of  $\approx 500$  keV.

Similarly, the bandhead  $K = \frac{1}{2}$  has the rotational sequence coupled to the above band with  $K = \frac{3}{2}$ . This spectrum is also well reproduced in Fig. 4 with the same deformation parameter. Thus it is evident that the model based on effective moment of inertia is quite successful in generating the energy spectrum of the two lowest-energy negative-parity bands in  $^{75}\text{Se}$ . Our treatment takes into account not only the Coriolis perturbation, but includes also the effects of mixing of states with same  $\Omega$  and differing  $j$  in the framework of the Nilsson formulation.

However, in spite of the present and previous [7–13] theoretical attempts to understand the structure of  $^{75}\text{Se}$ , the theoretical information about this nucleus is sparse. This may be due to lack, until recently, of relevant experimental information. The present investigation offers a detailed decay scheme of  $^{75}\text{Se}$  in which lifetimes of 17 states and spin values of many levels have been assigned for the first time. Multipole mixing ratios have also been predicted for a number of transitions. These values are

found to be in good agreement with previously reported [14] values. Accordingly, most of the proposed multipole mixing ratios represent weighted averages of previous and present results and can, therefore, be taken with greater confidence. This detailed information about lifetimes, multipole mixing ratios, and properties of electromagnetic transitions renders  $^{75}\text{Se}$  an attractive choice for testing theoretical models which are applicable in this region.

#### ACKNOWLEDGMENTS

The authors wish to thank the crew at the Chandigarh Cyclotron for providing an excellent proton beam. They also gratefully acknowledge the discussions with Prof. H. S. Hans. One of the authors (G.P.S.S.) acknowledges the financial support of the Council of Scientific and Industrial Research (CSIR). S.D.S. is grateful to the University Grants Commission (UGC) for funding the theoretical project.

---

\*Permanent address: Dept. of Physics, Panjab University, Chandigarh 160014, India.

†Deceased.

- [1] Y. K. Agarwal, C. V. K. Baba, S. M. Bharathi, S. K. Bhattacharjee, B. Lal, and Baldev Sahai, *Pramana* **3**, 243 (1974).
- [2] T. Sugimitsu, *Nucl. Phys.* **A224**, 199 (1974).
- [3] N. E. Sanderson and R. G. Summers-Gill, *Nucl. Phys.* **A261**, 93 (1976).
- [4] A. Shibuya, M. Dojo, T. Sugimitsu, and N. Kato, *Nucl. Phys.* **A301**, 15 (1978).
- [5] Y. Tokunaga, H. Seyfarth, O. W. B. Schult, S. Brant, V. Paar, D. Vretenar, H. G. Borner, G. Barreau, H. Faust, Ch. Hofmeyr, K. Schreckenbach, and R. A. Meyer, *Nucl. Phys.* **A430**, 269 (1984).
- [6] A. Coban, J. C. Willmott, J. C. Lisle, and G. Murray, *Nucl. Phys.* **A182**, 385 (1972).
- [7] N. E. Sanderson, *Nucl. Phys.* **A216**, 173 (1973).
- [8] L. S. Kisslinger and R. A. Sorenson, *Rev. Mod. Phys.* **35**, 853 (1963); L. S. Kisslinger and R. Kumar, *Phys. Rev. Lett.* **19**, 1239 (1967).
- [9] A. Goswami and O. Nalcioglu, *Phys. Lett.* **26B**, 353 (1968).
- [10] A. Goswami, D. K. McDaniels, and O. Nalcioglu, *Phys. Rev. C* **7**, 1263 (1973).
- [11] A. Kuriyama, T. Marumori, and K. Matsuyanagi, *Prog. Theor. Phys.* **45**, 784 (1971); **47**, 498 (1972).
- [12] W. Scholf and F. B. Malik, *Phys. Rev.* **176**, 1355 (1968).
- [13] A. I. Sherwood and A. Goswami, *Nucl. Phys.* **89**, 465 (1966).
- [14] A. R. Farhan and S. Rab, *Nucl. Data Sheets* **60**, 735 (1990).
- [15] J. T. Routti and S. G. Prussian, Lawrence Berkeley Radiation Laboratory Report No. UCLR-19452, 1969.
- [16] J. Lindhard, M. Scharff, and G. E. Schiott, *K. Dan. Vidensk. Selsk. Mat. Fys. Medd.* **33**, No. 14 (1963).
- [17] A. E. Blaugrund, *Nucl. Phys.* **88**, 501 (1966).
- [18] K. C. Jain, S. S. Datta, D. K. Avasthi, I. M. Govil, and V. K. Mittal, *Phys. Rev. C* **26**, 1310 (1982).
- [19] V. K. Mittal, D. K. Avasthi, and I. M. Govil, *J. Phys. G* **9**, 91 (1983).
- [20] E. Sheldon and V. C. Rogers, *Comput. Phys. Commun.* **6**, 99 (1973).
- [21] L. Rosen, J. G. Beery, and A. S. Goldhaber, *Ann. Phys. (N.Y.)* **34**, 96 (1965).
- [22] D. Wilmore and P. E. Hodgson, *Nucl. Phys.* **55**, 673 (1964).
- [23] F. G. Perey, *Phys. Rev.* **131**, 745 (1963).
- [24] P. A. Moldauer, *Nucl. Phys.* **47**, 65 (1963).
- [25] H. J. Rose and D. M. Brink, *Rev. Mod. Phys.* **39**, 306 (1967).
- [26] *Table of Isotopes*, 7th ed., edited by C. M. Lederer and V. S. Shirley (Wiley, New York, 1978).
- [27] J. P. Davidson, *Collective Models of the Nucleus* (Academic, New York, 1968), p. 183.